Fei Song,[1] Carmen Hurtado del Pozo,[1] Rosa Rosario,[1] Yu Shan Zou,[1] Radha Ananthakrishnan,[1] Xiaoyuan Xu,[2] Payal R. Patel,[3] Vivian M. Benoit,[3] Shi Fang Yan,[1] Huilin Li,[4] Richard A. Friedman,[5] Jason K. Kim,[3] Ravichandran Ramasamy,[1] Anthony W. Ferrante Jr.,[2] and Ann Marie Schmidt[1]

RAGE Regulates the Metabolic and Inflammatory Response to High-Fat Feeding in Mice

OBESITY STUDIES

In mammals, changes in the metabolic state, including obesity, fasting, cold challenge, and high-fat diets (HFDs), activate complex immune responses. In many strains of rodents, HFDs induce a rapid systemic inflammatory response and lead to obesity. Little is known about the molecular signals required for HFD-induced phenotypes. We studied the function of the receptor for advanced glycation end products (RAGE) in the development of phenotypes associated with high-fat feeding in mice. RAGE is highly expressed on immune cells, including macrophages. We found that high-fat feeding induced expression of RAGE ligand HMGB1 and carboxymethyllysine-advanced glycation end product epitopes in liver and adipose tissue. Genetic deficiency of RAGE prevented the effects of HFD on energy expenditure, weight gain, adipose tissue inflammation, and insulin resistance. RAGE deficiency had no effect on genetic forms of obesity caused by impaired melanocortin signaling. Hematopoietic deficiency of RAGE or treatment with soluble RAGE partially protected against peripheral HFD-induced inflammation and weight gain. These findings demonstrate that high-fat feeding induces peripheral inflammation and weight gain in a RAGE-dependent manner, providing a foothold in the pathways that regulate diet-induced obesity and offering the potential for therapeutic intervention.

The constellation of obesity, insulin resistance, and diabetes results from the integration of metabolic and inflammatory signals. When imbalances in caloric intake and energy expenditure contribute to obesity, disordered cross-talk among adipocytes, liver, brain, and skeletal muscle emerges, thereby eliciting cues that result in tissue recruitment of inflammatory cells. A consequence of inflammatory cell recruitment to key metabolic organs, particularly macrophage populations to visceral adipose tissue, is the derangement of the insulin signaling pathway, leading to impaired glucose and lipid homeostasis (1–5).

In this context, we hypothesized that receptor for advanced glycation end products (RAGE) might contribute to the pathogenesis of obesity and insulin resistance induced by a high-fat diet (HFD). RAGE is a multiligand receptor that recognizes stress and inflammatory signals, high mobility group box 1 (HMGB1), advanced glycation end products (AGEs), S100/calgranulins, lysophosphatidic acid, phosphatidyl serine, and ITGAM (6–11). RAGE is highly expressed on monocytes and macrophages, and its expression is further enhanced after immune activation or infection (12–16). Although seminal roles for RAGE in carbohydrate excess have been well studied, the regulation of RAGE signaling in the response to disturbances in lipid metabolism has been less well characterized.

---

[1]Diabetes Research Program, Division of Endocrinology, Department of Medicine, New York University School of Medicine, New York, NY

[2]Naomi Berrie Diabetes Center, Columbia University College of Physicians and Surgeons, New York, NY

[3]Program in Molecular Medicine and Division of Endocrinology, Diabetes and Metabolism, Department of Medicine, University of Massachusetts Medical School, Worcester, MA

[4]Departments of Population Health (Biostatistics) and Environmental Medicine, New York University School of Medicine, New York, NY

[5]Biomedical Informatics Shared Resource, Herbert Irving Comprehensive Cancer Center and Department of Biomedical Informatics, College of Physicians and Surgeons, Columbia University, New York, NY

High-fat feeding induces an inflammatory response in the liver, adipose tissue, and hypothalamus (17–19). The regulators of this inflammatory response remain largely obscure. We tested the hypothesis that high-fat feeding triggers production and accumulation of RAGE ligands in key metabolic tissues, which activate inflammatory signaling leading to obesity and insulin resistance. To test this model, we measured two key proinflammatory RAGE ligands in metabolic tissues and the effects of preventing RAGE activation in mice fed HFD. High-fat feeding induces RAGE ligand *Hmgb1* mRNA transcripts and carboxymethyllysine (CML)-AGE epitopes in liver and adipose tissue, and inhibition of RAGE by genetic or pharmacologic means has led to the unexpected result in mice that RAGE is required for the development of diet-induced obesity and its associated pathologies of insulin resistance and dyslipidemia. Furthermore, RAGE in bone marrow–derived cells accounts, at least in part, for these findings. The present data reveal fundamental metabolic sensing roles for RAGE and suggest that blockade of RAGE may prevent diet-induced obesity and metabolic dysfunction.

RESEARCH DESIGN AND METHODS

Animals and Diets

Homozygous RAGE null mice (C57BL/6 *Ager*$^{-/-}$ mice backcrossed >20 generations into C57BL/6J [The Jackson Laboratory, Bar Harbor, ME]) and their littermate RAGE-expressing controls were used. Ay mice (B6.Cg-A^y/J) (20) were purchased from The Jackson Laboratory and bred with homozygous RAGE null mice to generate C57BL/6 *Ay/a; Ager*$^{-/-}$ and littermate controls. All mice studied were male, had free access to water, and were subjected to 12-h light/dark cycles. At 6–8 weeks of age, mice were fed HFD with 60% of calories from lard (D12492; Research Diets, Inc., New Brunswick, NJ) or low-fat diet (LFD) with 13% of calories from fat (5053 PicoLab Rodent Diet 20; LabDiet, Brentwood, MO). Fat and lean masses were measured by dual-energy X-ray absorptiometry (DEXA) scanning. All animal procedures were approved by the Columbia University, New York University, and University of Massachusetts Medical School Institutional Animal Care and Use Committees and performed in accordance with the National Institutes of Health Animal Care Guidelines.

Energy Balance and Hyperinsulinemic-Euglycemic Clamp Studies

Metabolic studies were performed at the National Mouse Metabolic Phenotyping Center at UMass. Metabolic cages (TSE Systems, Inc., Midland, MI) were used in conscious mice to simultaneously measure energy expenditure through indirect calorimetry, food/water intake, and physical activity (21,22). Hyperinsulinemic-euglycemic clamps were performed in awake mice (23). An indwelling catheter was placed in the jugular vein 4–5 days before experiments. Following an overnight fast (~15 h), a 2-h hyperinsulinemic-euglycemic clamp was performed in conscious mice using a primed and continuous infusion of human insulin (Humulin; Eli Lilly and Company, Indianapolis, IN) at a rate of 15 pmol/kg/min to raise plasma insulin levels to within a physiologic range. Blood samples (20 μL) were collected at 20-min intervals for the immediate measurement of plasma glucose concentration; 20% glucose was infused at variable rates throughout the 2-h experiment to maintain plasma glucose at basal concentrations. Basal and insulin-stimulated whole-body glucose turnover was assessed with continuous infusion of [3-^{3}H] glucose (PerkinElmer Life and Analytical Sciences, Boston, MA) before (0.05 μCi/min) and throughout the clamps (0.1 μCi/min). To estimate insulin-stimulated glucose uptake in individual organs, 2-deoxy-D-[1-^{14}C] glucose (2[^{14}C]DG) (PerkinElmer) was administered as a bolus (10 μCi) 75 min after the start of the clamps. Blood samples were taken during and at the end of the clamps for measurement of plasma [3−^{3}H] glucose, ^{3}H$_2$O, and 2[^{14}C]DG concentrations and insulin. At the end of the clamp, mice were killed, and the organs were collected for multiple biochemical analyses, including measures of glycolysis and glucose production as previously described (24).

Measurement of Glucose, Lipid, Nonesterified Fatty Acids, and Insulin Levels in Fasted Mice

Blood glucose was measured with a FreeStyle blood glucose meter and strips (Abbott Diabetes Care Inc., Alameda, CA). Plasma cholesterol concentrations were measured with standard assays (Infinity Cholesterol Reagent; Fisher Diagnostics, Middletown, VA) or (Cholesterol E; Wako Diagnostics, Richmond, VA). The concentration of serum nonesterified fatty acids was measured using a colorimetric assay NEFA C test kit (Wako Diagnostics). Blood insulin concentrations were measured by ELISA (ALPCO Diagnostics, Salem, NH) (Fig. 8D) or by rat ultrasensitive ELISA (cross-reacts with murine insulin) (Fig. 2B) (Mercodia Inc., Winston-Salem, NC).

Glucose and Insulin Tolerance Tests

After baseline collection of blood, glucose 2 g/kg or insulin (Eli Lilly and Company) 0.75 units/kg was injected intraperitoneally. Serial blood glucose analysis was performed through 120 min postinjection (25).

Soluble RAGE (sRAGE) (human) was prepared, purified, and rendered free of endotoxin (16), and 100 μg/day i.p. was administered to mice. Vehicle consisted of equal volumes of PBS.

Real-Time Quantitative PCR

Total RNA was extracted from liver or epididymal fat tissue using the RNeasy lipid kit (Qiagen, Hilden, Germany). cDNA was synthesized with MultiScribe reverse transcriptase (Applied Biosystems, Foster City, CA). Real-time quantitative PCR was performed using the TaqMan method (50°C for 2 min, 95°C for 10 min, and 40 cycles of 95°C for 15 s and 60°C for 1 min) with premade primer sets (Applied Biosystems). The relative abundance of

transcripts was normalized according to the expression of 18S rRNA or β-actin using the ΔΔCt method and, where indicated, according to the expression of *Emr1* macrophage-specific marker in perigonadal adipose tissue (PGAT). Supplementary Table 1 lists the specific primers and probes.

Preparation of Visceral Fat Suspension and Fluorescence-Activated Cell Sorting

Epididymal fat pads were excised from male C57BL/6 mice fed HFD, weighed, and rinsed three times in PBS containing low endotoxin BSA and EDTA (1 mm). Tissue suspensions were subjected to centrifugation at 500*g* for 5 min and then collagenase treated (1 mg/mL) (Sigma-Aldrich, St. Louis, MO) for 30 min at 37°C with shaking. Cell suspensions were passed through a 100-μm filter and centrifuged at 500*g* for 5 min. Adipocyte fractions were collected into QIAzol (Qiagen, Valencia, CA) for RNA extraction. Stromal vascular cell fraction pellets were then incubated with erythrocyte lysis buffer (eBioscience, San Diego, CA) for 5 min before centrifugation (300*g* for 5 min) and resuspended in fluorescence-activated cell sorting buffer. Stromal vascular cell fractions were incubated with Fc Block (BD Biosciences, San Jose, CA) for 20 min at 4°C before staining with fluorescently labeled primary antibodies. The antibodies used were as follows: anti-mouse CD45 Alexa Fluor 700 and anti-mouse F4/80 antigen PerCP-Cyanine5.5. Cells were sorted using a MoFlo sorter (Beckman Coulter, Brea, CA) into RTL buffer (Qiagen).

Adipocyte Measurements and Expression of F4/80 and Cd11c$^+$ Cells in PGAT

Immunohistochemistry was performed on 4-μm-thick formalin-fixed, paraffin-embedded PGAT using mouse-Cd11c, clone 5D11 (Novocastra/Leica Biosystems, Newcastle upon Tyne, U.K.) and rat F4/80, clone CI:A3-1 (Abcam, Cambridge, MA). Following deparaffinization, for detection of Cd11c, heat-induced epitope retrieval was performed in a microwave oven in 10 mmol/L sodium citrate buffer (pH 6.0) for 20 min. Antibody incubation and detection were carried out at 40°C on a NexES instrument (Ventana Medical Systems, Tucson, AZ) using the manufacturer's reagent buffer and detection kits. Endogenous peroxidase activity was blocked with hydrogen peroxide. F4/80 antigen retrieval was performed using alkaline endopeptidase (Ventana Medical Systems) for 10 min. Anti-Cd11c and F4/80 antibodies were diluted 1:50 and 1:40, respectively, in Dulbecco's phosphate-buffered saline (Life Technologies, Grand Island, NY). Primary antibodies were incubated overnight at room temperature. Cd11c was detected using biotinylated horse anti-mouse antibody, diluted 1:400. F4/80 was detected using mouse-absorbed, biotinylated rabbit anti-rat antibody diluted 1:300 (Vector Laboratories, Burlingame, CA). Both secondary antibodies were incubated for 30 min followed by streptavidin-horseradish peroxidase conjugate. The complex was visualized with 3,3-diaminobenzidene

and enhanced with copper sulfate. Slides were washed in distilled water, counterstained with hematoxylin, dehydrated, and mounted with permanent media. Appropriate positive and negative controls were included in the studies. An observer naïve to the experimental conditions performed quantification of F4/80 or Cd11c content in four sections obtained from each adipose tissue pad in five mice per group. The total number of nuclei and the number of nuclei of F4/80-expressing cells were counted for each field. The fraction of F4/80-expressing cells for each sample was calculated as the sum of the number of nuclei of F4/80-expressing cells divided by the total number of nuclei in sections of a sample (25). The same procedure was used to measure the fraction of CD11c-expressing cells in PGAT. Mean adipocyte size in pixels was determined using Image-Pro Analyzer 7.0 (Media Cybernetics, Inc., Silver Spring, MD), measuring a minimum of 400 cells per sample and reported in square micrometers.

Immunohistochemical Detection of Microglia

Brains were retrieved from the indicated mice. One midline sagittal section of each brain was formalin fixed and paraffin embedded. Immunohistochemistry was performed on 4-μm-thick sections using polyclonal rabbit-anti-ionized calcium-binding adapter molecule 1 (Iba1, 019-19741; Wako Diagnostics). Antibody incubation and detection were carried out at 40°C on a NexES instrument (Ventana Medical Systems) using the manufacturer's reagent buffer, detection kit, and instructions. Appropriate positive and negative controls were included with the study sections. Stained slides were scanned using a Leica SCN400 F whole-slide scanner. All quantitative analyses were performed on a 40× image of one midline sagittal section per mouse, and the observers were naïve to the experimental conditions. The area of the hypothalamus was manually outlined with reference to a hematoxylin-eosin staining of the adjacent section. Iba1 immunoreactive microglia were manually counted throughout the hypothalamus section, and results were expressed as number of cells per square millimeter in five mice per experimental condition.

Bone Marrow Transplantation

Six-week-old male C57BL/6J recipient mice received two doses of 600 rad from a ^{137}Cs source (Gammacell 40; Atomic Energy of Canada Ltd., Mississauga, ON, Canada) over 4 h. Bone marrow was collected from the femurs and tibias of C56BL/6J or RAGE null donor mice into Hanks' balanced salt solution. Cells (5×10^6) were injected into the recipient's lateral tail vein 4 h after the second irradiation. The recipient mice were maintained in a pathogen-free facility and fed standard chow; for 2 weeks, water was supplemented with 0.5 mL/L 10% Baytril (Bayer Corporation, Shawnee Mission, KS). Four weeks after transplantation, mice were fed HFD or LFD until euthanasia.

Statistical Analysis

The mean ± SEM is reported. For comparison between two groups, data were analyzed by the two-tailed Student

t test using Microsoft Excel software (Microsoft Corporation, Redmond, WA). For comparisons among four groups, ANOVA was accomplished with a one-way ANOVA followed by an unpaired, two-tailed Student *t* test for *P* value using SPSS Advanced Statistics version 20.0 software (IBM Corporation, Chicago, IL). $P < 0.05$ was considered statistically significant. To test the association of *Ager* genotype and physical activity with body weight, linear regression analysis was performed using SAS 9.3 software (SAS Institute, Cary, NC).

RESULTS

To test the hypothesis that RAGE contributes to inflammatory and metabolic responses to high-fat feeding, we asked whether HFD affects the concentration of two prototypic proinflammatory RAGE ligands in the liver and PGAT, two key metabolic tissues. *Hmgb1* mRNA transcripts were significantly higher in the livers and PGAT of mice fed HFD versus LFD ($P < 0.00001$) (Fig. 1*A* and *B*). Accumulation of CML-AGE epitopes was significantly higher in the PGAT and liver tissue of mice fed HFD versus LFD ($P < 0.05$) (Supplementary Fig. 1*A* and *B*). This significant rise in two key proinflammatory RAGE ligands in the liver and PGAT prompted us to test the effects of RAGE on the response to HFD. Homozygous RAGE null and wild-type (WT) littermate mice were fed LFD or HFD beginning at age 6 weeks. There were no baseline differences in body mass among the four groups of mice (Fig. 1*C*). *Ager* genotype had no effect on weight gain in LFD-fed mice (Fig. 1*C*). In contrast and unexpectedly, on HFD, RAGE null mice were protected from weight gain experienced by the WT mice (26.7 ± 2.0 vs. 39.3 ± 1.75 g, respectively; $P < 0.001$) (Fig. 1*C*).

Obesity increases both fat and lean mass in human subjects and in most animal models. To determine whether the difference in body mass was due to differences in fat or lean mass or both, we performed DEXA scanning. There was no difference in body composition between LFD-fed WT and RAGE null mice. As expected, high-fat feeding increased both lean and fat mass in WT mice ($P < 0.05$); both lean and fat mass were significantly lower in HFD-fed RAGE null animals ($P < 0.005$) (Fig. 1*D*). Consistent with reduced adiposity, HFD-fed RAGE null mice displayed smaller adipocytes than WT littermates, although the reduction in size was smaller than would be predicted if *Ager* genotype only reduced adipose hypertrophy ($P < 0.05$) (Fig. 1*E*). Thus, RAGE does not play a measurable role in weight regulation or body composition in LFD-fed animals but is required for the development of obesity in high-fat feeding.

We next measured the effect of *Ager* genotype on glycemia and insulin sensitivity in high-fat feeding. There was no difference in fasting blood glucose levels in LFD-fed WT versus RAGE null mice. After 3 months of HFD, fasting blood glucose in WT mice was higher than in mice fed LFD ($P < 0.0005$) (Fig. 2*A*). On HFD, blood glucose was significantly lower in RAGE null mice than in WT mice ($P = 0.001$) (Fig. 2*A*).

To determine whether deletion of RAGE altered insulin sensitivity, we measured plasma insulin levels and performed insulin tolerance tests. There were no significant differences in fasting plasma insulin concentrations among the four groups of mice after 3 months of diet (Fig. 2*B*). In mice fed LFD, RAGE null mice were slightly more sensitive to insulin challenge than WT mice at age 6 weeks ($P = 0.05$) (Fig. 2*C*). After 3 months of HFD, RAGE null mice were significantly more insulin sensitive than WT mice ($P < 0.0005$) (Fig. 2*D*). There was no difference in insulin sensitivity between WT and RAGE null mice fed LFD at this age. Levels of *Slc2a4* mRNA transcripts (encoding GLUT4) were significantly higher in the PGAT of RAGE null mice fed HFD versus WT mice fed HFD ($P < 0.0002$) (Fig. 2*E*). Consistent with an overall more favorable metabolic phenotype, RAGE null mice had a lower concentration of plasma cholesterol than did WT mice after 3 months of HFD ($P < 0.01$) (Fig. 2*F*), and the circulating concentration of fasting nonesterified fatty acids, an indirect measure of lipolysis and insulin sensitivity, was >60% lower in RAGE null mice fed HFD than in WT mice ($P < 0.01$) (Fig. 2*G*).

We performed hyperinsulinemic-euglycemic clamp experiments to further probe the state of insulin sensitivity and its relationship to RAGE. Basal glucose levels were similar in LFD-fed WT and RAGE null mice, but after 8 weeks of HFD, they were significantly lower in RAGE null than in WT mice ($P < 0.02$) (Fig. 3*A*). During the clamp, plasma glucose concentrations did not differ between WT or RAGE null mice fed either diet (Fig. 3*B*). In both LFD- and HFD-fed RAGE null mice, significantly higher glucose infusion rates were required during the clamp to maintain euglycemia compared with WT mice ($P < 0.01$) (Fig. 3*C*). Although glucose turnover was ~10% higher in RAGE null versus WT mice fed LFD ($P = 0.03$), an ~28% higher glucose turnover rate was observed in RAGE null versus WT mice fed HFD ($P = 0.01$) (Fig. 3*D*). No differences in whole-body glycolysis were observed between RAGE null and WT mice fed either LFD or HFD (Fig. 3*E*), but whole-body glycogen synthesis rates were ~50% higher in RAGE null than in WT mice fed HFD ($P = 0.04$); no differences were observed between the two groups of mice fed LFD (Fig. 3*F*).

The finding of roles for RAGE in insulin sensitivity led us to test hepatic insulin action. Although there were no differences in basal hepatic glucose production between RAGE null and WT mice fed LFD or HFD (Fig. 3*G*), clamp hepatic glucose production was significantly reduced by RAGE deletion in mice fed either LFD or HFD. In mice fed LFD, RAGE null mice displayed ~89% lower hepatic glucose production than WT mice ($P = 0.02$) and 100% lower hepatic glucose production in high-fat feeding than WT mice ($P = 0.07$) (Fig. 3*H*). Hepatic insulin action was ~19% higher in RAGE null mice fed LFD than in WT mice ($P = 0.07$) and ~30% higher in RAGE null mice fed HFD than in WT mice ($P = 0.04$) (Fig. 3*I*).
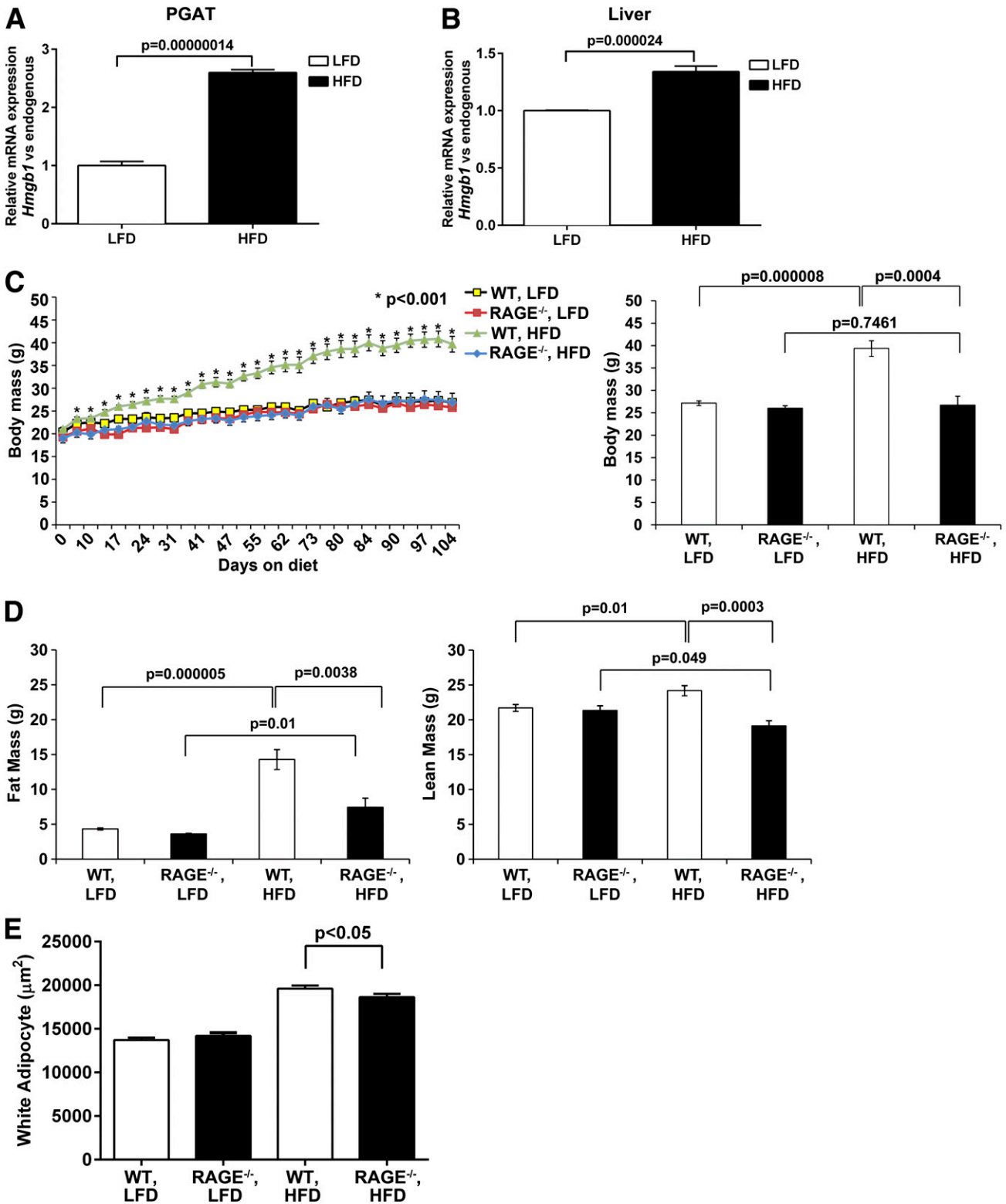
Figure 1—Mice devoid of RAGE are resistant to HFD-induced obesity. *A* and *B*: Two weeks after induction of LFD or HFD, PGAT (*A*) and liver tissue (*B*) were retrieved and subjected to real-time quantitative PCR for detection of *Hmgb1* mRNA transcripts (*A* and *B*) (*n* = 6 mice/group). *C*: WT and RAGE null male mice were fed LFD or HFD, and body mass was measured. The *left* panel shows time course studies, and the *right* panel shows mean body mass at the end of the study (*n* = 7–8 mice/group). *P < 0.001 comparing WT vs. RAGE null mice fed HFD. *D*: Body composition. One week before the end of the study in panel *C*, fat (*left*) and lean (*right*) mass were determined by DEXA scanning (*n* = 7–8 mice/group). *E*: WT and RAGE null mice fed LFD or HFD for 3 months were killed, and PGAT was retrieved for determination of adipocyte size (*n* = 4 mice/group).
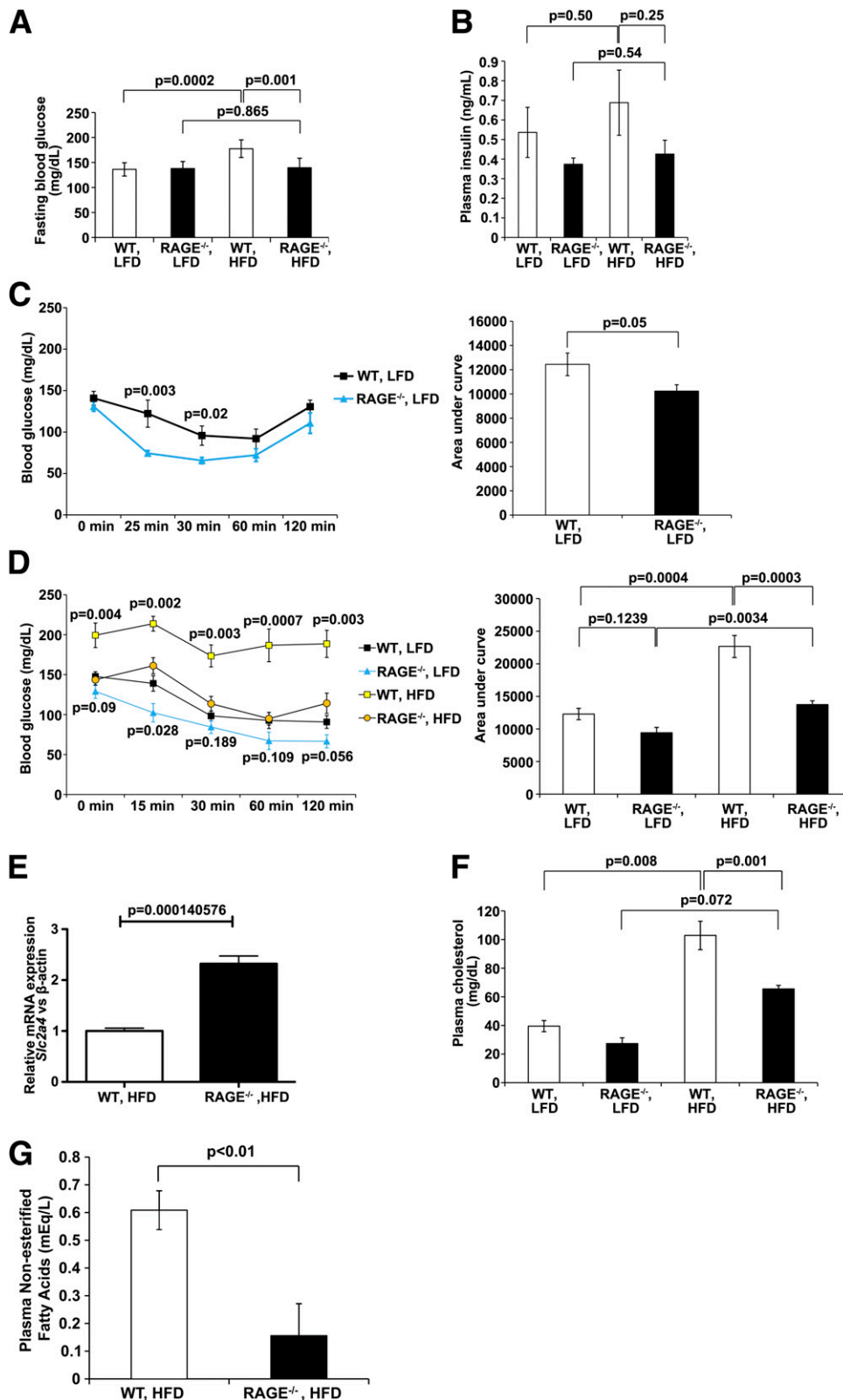
Figure 2—Mice devoid of RAGE are resistant to HFD-induced hyperglycemia and insulin intolerance. *A*: Concentration of fasting blood glucose was measured. *B*: Fasting plasma insulin concentrations were measured by ELISA. *C* and *D*: An insulin tolerance test was performed in LFD-fed mice (*C*) and LFD- and HFD-fed mice (*D*). *E*: Levels of *Slc2a4* mRNA transcripts were determined in PGAT of WT vs. RAGE null mice fed HFD. *F* and *G*: Fasting plasma cholesterol (*F*) and nonesterified fatty acid (*G*) concentrations were measured in WT and RAGE null mice fed LFD or HFD. $n = 7$–8 mice per group studied in *A*, *C*, *D*, and *F*; $n = 3$–4 in *B*; $n = 6$ mice/group in *E*; and $n = 5$ mice/group in *G*. Studies in *A*, *B*, and *D–G* were performed at the end of the study (i.e., after 3 months of diet). Studies in *C* were performed at age 6 weeks.
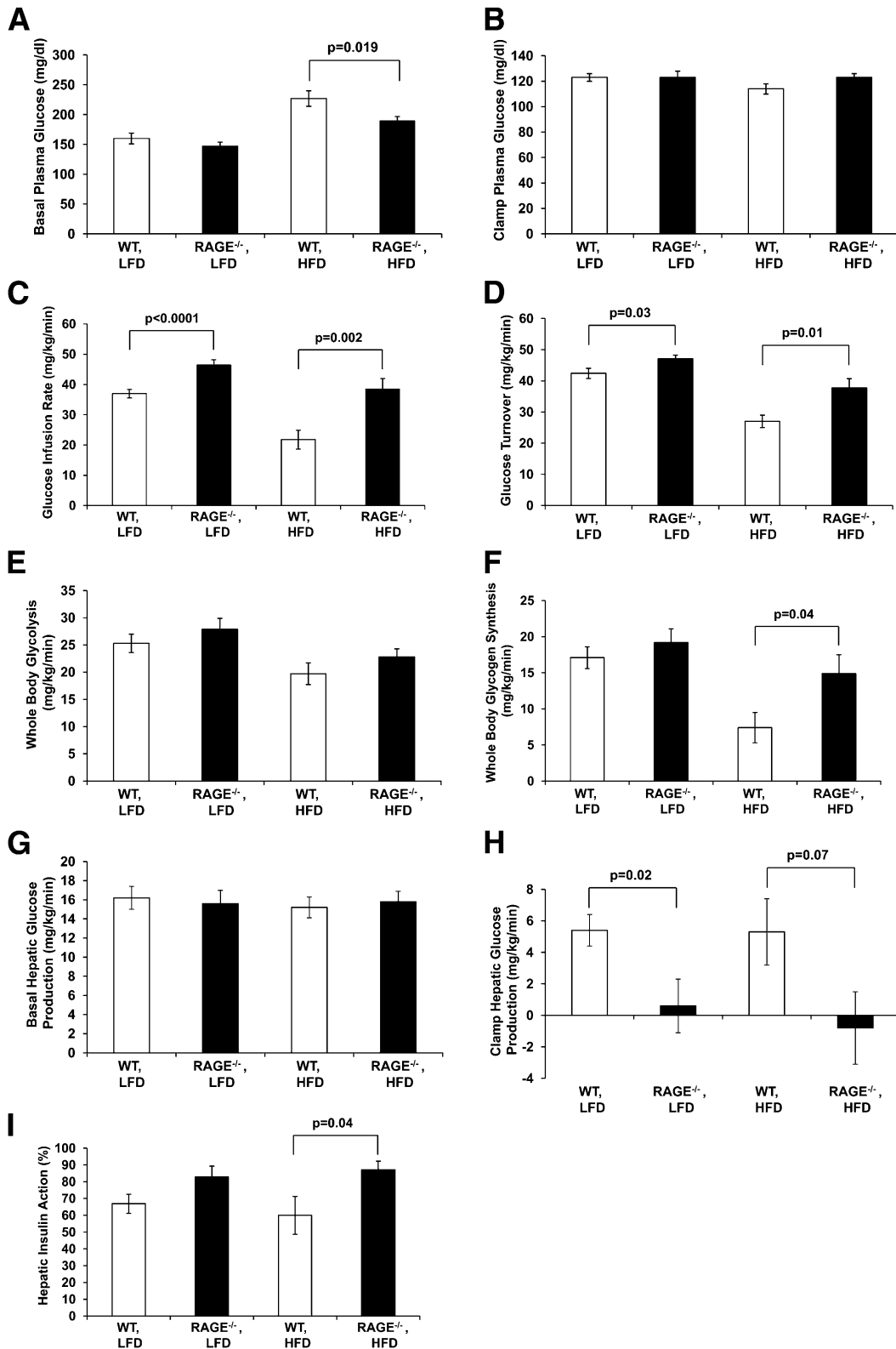
Figure 3—Mice devoid of RAGE had increased sensitivity to insulin. After 8 weeks of LFD or HFD, WT and RAGE null mice were subjected to 2-h hyperinsulinemic-euglycemic clamps and glucose metabolism experiments, and the following were studied: basal and clamp concentrations of plasma glucose (*A* and *B*), glucose infusion rate (*C*), glucose turnover rate (*D*), whole-body glycolysis (*E*), whole-body glycogen synthesis (*F*), basal and clamp hepatic glucose production (*G* and *H*), and percent hepatic insulin action (*I*). Number of mice per group were as follows: WT, LFD, $n = 12$; RAGE null, LFD, $n = 10$; WT, HFD, $n = 9$; and RAGE null, HFD, $n = 10$.

These data led us to ask whether RAGE was necessary for the development of obesity per se or was specifically required for the metabolic effects of high-fat feeding. The modest reduction in adipocyte size in RAGE null versus WT mice fed HFD (~5%) could not explain the reduced adiposity and raises the possibility that adipose tissue hyperplasia was fundamentally impaired in RAGE null mice. To answer this question, we intercrossed the RAGE null allele ($Ager^{-/-}$) into an A^y/a (agouti) background. In C57BL/6J A^y/a mice, impairment of central melanocortin signaling leads to hyperphagia and the development of obesity, even in low-fat–fed animals. There was no significant difference in body mass in A^y/a mice expressing or lacking RAGE, and there were no differences in lean or fat mass between A^y/a mice expressing or lacking RAGE by DEXA scan (Supplementary Fig. 2A and B). Hence, RAGE null mice may undergo hypertrophy and develop obesity, but they are specifically impaired in their metabolic response to high-fat feeding.

In response to HFD, obesity-susceptible strains of mice, including C57BL/6J, reduce energy expenditure (26). To test whether RAGE deficiency attenuated the effects of high-fat feeding on energy expenditure and substrate use, we measured food intake and used an indirect calorimetry system to measure O_2 consumption (VO_2) and CO_2 production (VCO_2). There were no differences in caloric intake among RAGE null mice and WT controls (Fig. 4A). At baseline on LFD, during 24 h and the 12-h dark cycle, RAGE null animals had slightly higher VO_2 than WT mice ($P < 0.05$) (Fig. 4B). As expected, after 3 and 6 weeks of HFD, VO_2 was reduced in WT mice. Consistent with RAGE being required for the reduced energy expenditure associated with high-fat feeding, RAGE null mice had higher VO_2 during both light and dark periods than WT controls (Fig. 4B). There was no difference in VCO_2 at baseline (day or night periods) between WT and RAGE null mice fed LFD. After 3 and 6 weeks of HFD, RAGE null mice had significantly higher VCO_2 during day and night periods than did WT controls (Fig. 4C). The respiratory exchange ratio (RER) did not differ among any of the groups (Fig. 4D). Physical activity was monitored over a 3-day period per time period; as expected, HFD feeding lowered physical activity in WT mice compared with LFD (Fig. 4E). Physical activity was higher in RAGE null vs. WT mice at baseline, 3 weeks, and 6 weeks of HFD but was lower in RAGE null mice fed HFD versus LFD. Further statistical analyses were performed to discern the association among physical activity, $Ager$ genotype, and body weight at 6 weeks of HFD. Without considering $Ager$ status, physical activity alone is not statistically significantly associated with body weight ($P = 0.11$). When we tested the association of physical activity and $Ager$ status together with body weight, we found that physical activity is not associated with weight gain on HFD ($P = 0.45$). However, $Ager$ genotype is significantly associated with body weight ($P = 0.03$). These analyses support that physical activity does not confound the protective effect of $Ager$ deficiency on protection against obesity in high-fat feeding.

To further probe roles for RAGE action on physical activity, we treated LFD-fed mice with the RAGE ligand decoy sRAGE. As shown in Supplementary Fig. 3, sRAGE, which does not cross the blood-brain barrier, imparted no effect on physical activity and no effect on energy expenditure. Furthermore, in WT mice subjected to lethal irradiation and reconstitution with either RAGE null or WT bone marrow, although physical activity was higher in mice reconstituted with RAGE null bone marrow, there was no effect on energy expenditure (Supplementary Fig. 4). These data suggest that the mechanisms by which RAGE modulates physical activity are complex and may be regulated, at least in part, by central signals.

Furthermore, in the context of metabolic phenotype, RAGE null mice fed HFD had significantly higher body temperature than did WT littermates (Supplementary Fig. 5). We measured mRNA transcripts for $Ucp1$ in the brown adipose tissue (BAT) of WT and RAGE null mice fed HFD versus LFD (Supplementary Fig. 6). In high-fat feeding, $Ucp1$ mRNA transcripts did not differ in BAT between WT and RAGE null mice. In low-fat feeding, $Ucp1$ mRNA transcripts were one-half that in BAT of RAGE null versus WT mice ($P = 0.001$). A trend toward lower levels of $Ucp1$ mRNA transcripts was observed in BAT of WT mice fed HFD versus LFD. In contrast, in RAGE null mice BAT, significantly higher levels of $Ucp1$ mRNA transcripts were observed in HFD versus LFD ($P = 0.015$) (Supplementary Fig. 6). Taken together, these findings suggest that in response to HFD challenge, RAGE null mice significantly increase their energy expenditure in the absence of increased food consumption and without increasing their physical activity compared with LFD.

Studies have suggested that M2 polarized macrophages in adipose tissue are associated with catabolic function and energy expenditure (27). Given the established expression of RAGE on macrophage populations, we tested the relative expression of RAGE in F4/80-expressing macrophages versus adipocytes in the PGAT of HFD-fed mice. As shown in Supplementary Fig. 7, RAGE was highly expressed in the F4/80-expressing fraction versus adipocyte fractions in PGAT in high-fat feeding. Hence, we hypothesized that RAGE might contribute to an altered macrophage content and polarization state in PGAT, thereby contributing to altered energy expenditure. As expected, the expression of $F4/80$ $(Emr1)$ mRNA transcripts was higher in WT mice fed HFD than in lean mice fed LFD (Fig. 5A), and consistent with a reduction in adiposity, the expression of $Emr1$ in PGAT of HFD-fed RAGE null mice was reduced >90% compared with HFD-fed WT mice ($P = 0.001$). Consistent with these data, immunohistochemistry with anti-F4/80 IgG revealed increased numbers of F4/80-expressing cells in PGAT of WT mice fed HFD versus LFD, which was significantly reduced by RAGE deletion ($P < 0.05$) (Fig. 5B and D–G). Furthermore, immunohistochemistry with anti-Cd11c
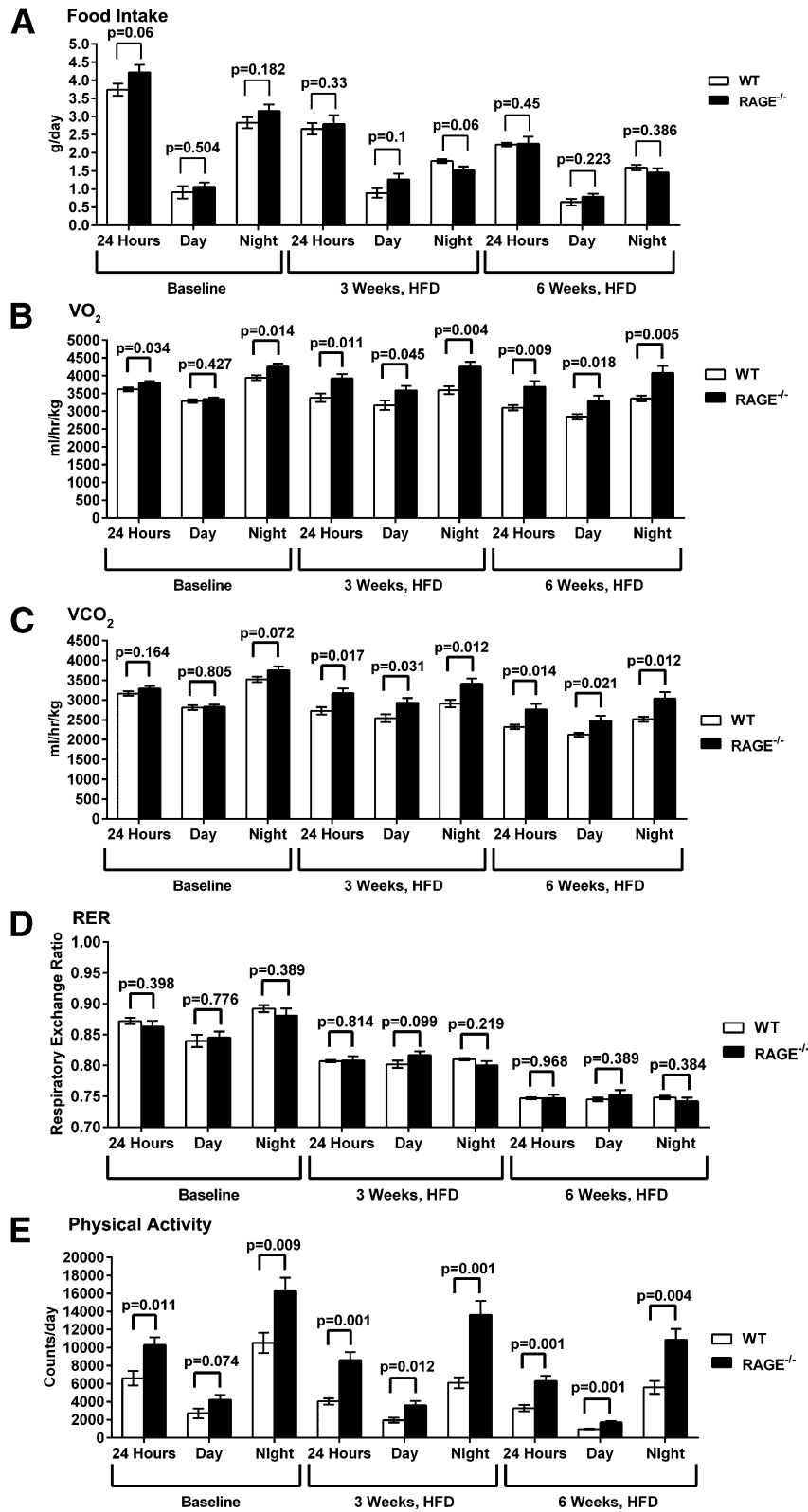
Figure 4—RAGE null mice displayed higher energy expenditure than WT mice. *A*: Food consumption was monitored at baseline and 3 and 6 weeks post-HFD. *B–E*: Mice were placed in metabolic chambers for assessment of VO_2 (*B*), VCO_2 (*C*), RER (*D*), and physical activity (*E*) at baseline, 3 weeks HFD, and 6 weeks HFD. The *y*-axes in all panels have an identical scale across the three time points. *n* = 6 mice/group.
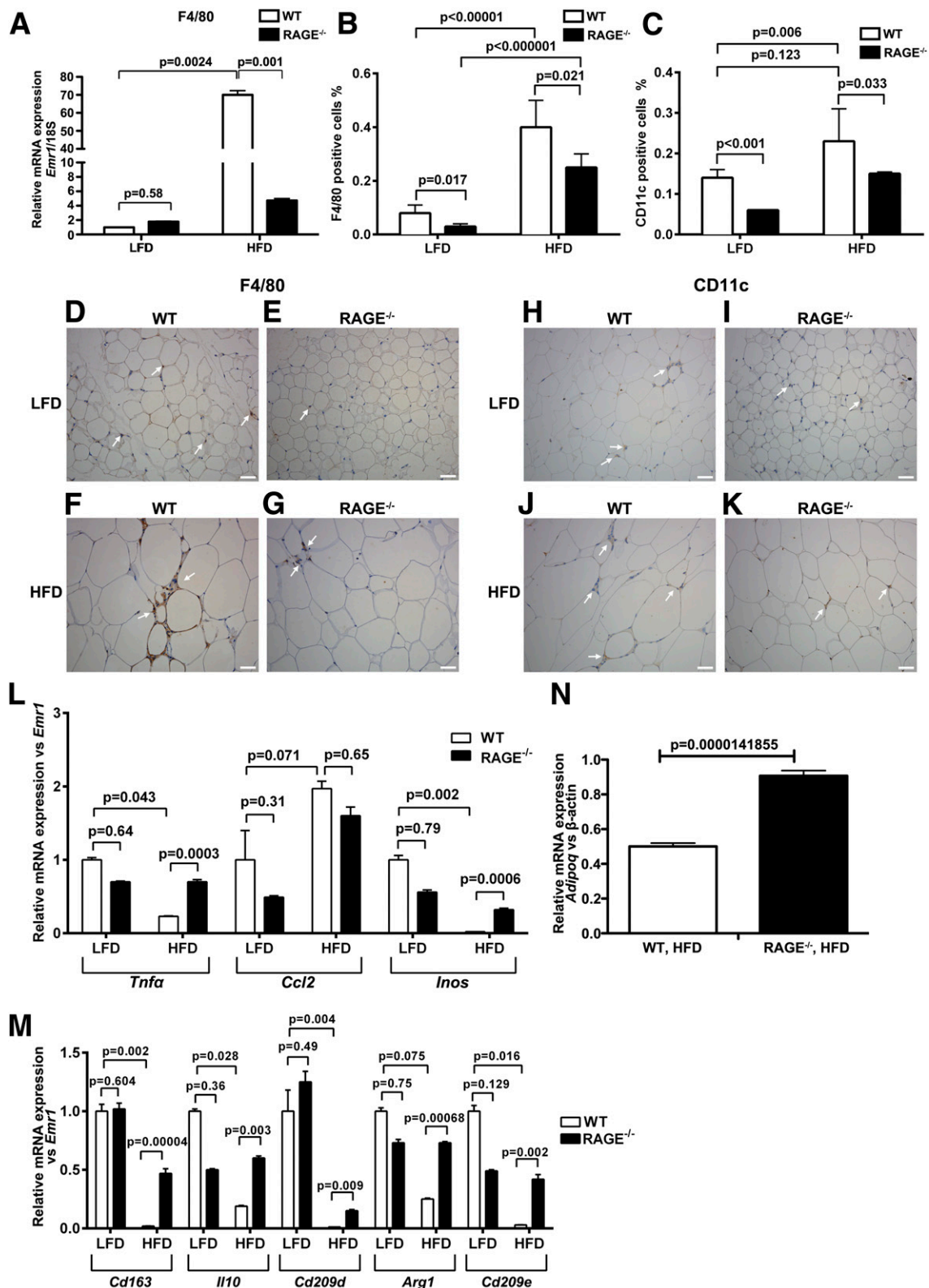
Figure 5—Deletion of RAGE reduces macrophage *Emr1* mRNA transcripts and F4/80- and Cd11c-expressing cells and modulates M1/M2 polarization in PGAT in HFD feeding. WT and RAGE null mice were fed LFD or HFD for 3 months; at the end of that time, PGAT was retrieved and subjected to real-time quantitative PCR for detection of *Emr1* mRNA transcripts (*A*). *B* and *C*: After 3 months of LFD or HFD feeding, PGAT was retrieved and subjected to immunohistochemistry with anti-F4/80 (*B*) or anti-Cd11c IgG (*C*) (*n* = 4 mice/group). *D–K*: Representative images from WT and RAGE null PGAT are shown for F4/80 (*D–G*) and Cd11c (*H–K*) immunoreactivity (scale bar: 40 μm). Arrows highlight F4/80- or Cd11c-expressing cells. *L* and *M*: mRNA transcripts were determined for the indicated M1 (*L*) and M2 (*M*) macrophage markers and compared directly to absolute levels of *Emr1* mRNA transcripts in PGAT after the 3-month diets (*n* = 6 mice/group). *N*: Levels of PGAT *Adipoq* mRNA transcripts were determined in WT vs. RAGE null mice fed HFD (*n* = 5 mice/group).

IgG revealed significantly higher Cd11c-expressing cells in WT PGAT in high-fat feeding, which was significantly lower in RAGE null mice fed HFD ($P < 0.05$) (Fig. 5C and H–K). We next assessed whether the polarization profile of the PGAT was skewed toward an M1 or M2 state and compared the expression of genes typical of each state relative to *Emr1* expression. The effect of RAGE genotype on M1 genes was not consistent. Deletion of RAGE in mice fed HFD resulted in no significant effect on prototypic M1 gene *Ccl2* relative to *Emr1* mRNA expression, but the expression of the classical activation markers *Tnf* and *Inos* mRNA transcripts relative to *Emr1* was significantly higher in HFD-fed RAGE null mice than in HFD-fed WT mice ($P < 0.001$) (Fig. 5L). In contrast, levels of mRNA transcripts of M2 macrophage polarization markers *Cd163*, *Il10*, *Arg1*, *Cd209d*, and *Cd209e* were all consistently higher in RAGE null mice than in WT mice fed HFD ($P < 0.05$) (Fig. 5M). Furthermore, in PGAT of RAGE null mice fed HFD, *Adipoq* mRNA transcripts (encoding adiponectin) were significantly higher than those observed in WT mice ($P < 0.00002$) (Fig. 5N). Taken together, these data indicate that overall PGAT inflammation was lower in HFD-fed RAGE null versus WT mice.

Other studies suggested that high-fat feeding incites hypothalamic inflammation (19); therefore, we performed immunohistochemistry for detection of Iba1 epitopes, a marker of activated microglia, in the hypothalamus of WT and RAGE null mice fed HFD. As shown in Supplementary Fig. 8, high-fat feeding induced a trend toward higher levels of Iba1+ cells in the hypothalamus of WT mice fed HFD versus LFD ($P = 0.06$). Of note and analogous to inflammatory cell infiltration in PGAT of LFD-fed RAGE null mice, on LFD, RAGE null mice displayed significantly lower numbers of Iba1+ cells in the hypothalamus than did WT mice fed LFD ($P = 0.005$). A nonstatistically significant trend to lower numbers of Iba1+ cells was noted in the hypothalamus of RAGE null versus WT mice fed HFD; the numbers of Iba1+ cells in RAGE null hypothalamus in high-fat feeding were higher than those in the hypothalamus of RAGE null mice fed LFD ($P = 0.002$) (Supplementary Fig. 8).

Thus, assessing whether hematopoietic immune cells could drive the obesity-protecting effects of RAGE deficiency and the M2-skewed phenotype of adipose tissue in high-fat feeding was the next logical step. We irradiated WT mice and reconstituted them with bone marrow derived from RAGE-expressing or RAGE null mice. Compared with HFD-fed mice reconstituted with WT bone marrow, recipients of RAGE null bone marrow gained weight at a significantly slower rate than WT mice. After 5 months on HFD, mice that lacked RAGE specifically in hematopoietic cells weighed 19% less than mice with intact RAGE (33.5 ± 3.1 vs. 41.6 ± 4.7 g; $P < 0.05$) (Fig. 6A). The HFD-fed recipients of RAGE null bone marrow were also more glucose tolerant than the mice receiving WT bone marrow and fed HFD ($P < 0.05$)

(Fig. 6B). Despite a reduced body mass, HFD-fed mice with hematopoietic deficiency of RAGE displayed modest, but significantly higher daily food consumption compared with mice with intact RAGE ($P = 0.01$) (Fig. 6C). Plasma concentration of total cholesterol was higher in HFD-fed mice that lacked hematopoietic RAGE than in those with intact RAGE ($P < 0.05$) (Fig. 6D). Adipocyte size did not differ between recipients of WT versus RAGE null bone marrow fed HFD (Fig. 6E).

We next assessed inflammatory cell infiltration into PGAT and M1/M2 polarization. Consistent with the findings in whole-body RAGE-deficient mice, *Emr1* mRNA transcripts were significantly higher in WT recipients of WT bone marrow after 3 months of HFD versus LFD. Deletion of bone marrow RAGE in the HFD-fed mice resulted in significantly lower *Emr1* mRNA transcript levels versus the WT bone marrow recipients ($P = 0.02$) (Fig. 7A). In PGAT, recipients of WT bone marrow fed HFD displayed significantly higher numbers of F4/80-expressing cells by immunohistochemistry; this was significantly lower in PGAT of recipients of RAGE null bone marrow fed HFD ($P = 0.002$) (Fig. 7B and D–G). Numbers of Cd11c-expressing cells were significantly lower in the PGAT of recipients of RAGE null bone marrow versus recipients o WT bone marrow fed HFD ($P < 0.05$) (Fig. 7C and H–K). Consistent with findings in mice globally devoid of RAGE, mice receiving RAGE null versus WT bone marrow fed HFD displayed significantly higher levels of M1 polarization mRNA transcripts *Tnf*, *Ccl2*, and *Inos* (Fig. 7L). In contrast and analogous to findings in whole-body RAGE deletion, WT recipients of RAGE null bone marrow fed HFD displayed significantly higher levels of *Il10* and *Arg1* mRNA transcripts than recipients of WT bone marrow; similar trends were observed for *Cd209d* and *Cd209e* (Fig. 7M).

Finally, because the data revealed increased concentrations of RAGE ligands HMGB1 and CML-AGEs in the liver and PGAT after induction of HFD, we tested the hypothesis that administration of the ligand-binding decoy, sRAGE, might affect the consequences of HFD feeding. WT mice were treated with sRAGE 100 μg/day i.p., beginning immediately at the time of HFD feeding at age 6 weeks. Control mice were treated with equal amounts of vehicle PBS. By 18 weeks of HFD, mean body mass was 34.0 ± 5.3 vs. 42.0 ± 1.7 g in sRAGE versus vehicle-treated mice, respectively ($P < 0.05$) (Fig. 8A). The benefits of sRAGE were specific to HFD feeding because sRAGE had no effect on body mass in mice fed LFD (Fig. 8B).

Fasting blood glucose levels were not different between LFD-fed vehicle versus sRAGE-treated mice but were significantly lower in the sRAGE-treated mice fed HFD versus vehicle-treated mice ($P < 0.01$) (Fig. 8C). HFD resulted in significantly higher insulin levels than LFD in the WT mice ($P < 0.05$) and a trend toward lower insulin levels in sRAGE- versus vehicle-treated HFD-fed mice (Fig. 8D). Food consumption was not different in HFD-fed mice treated with sRAGE vs. vehicle (Fig. 8E).
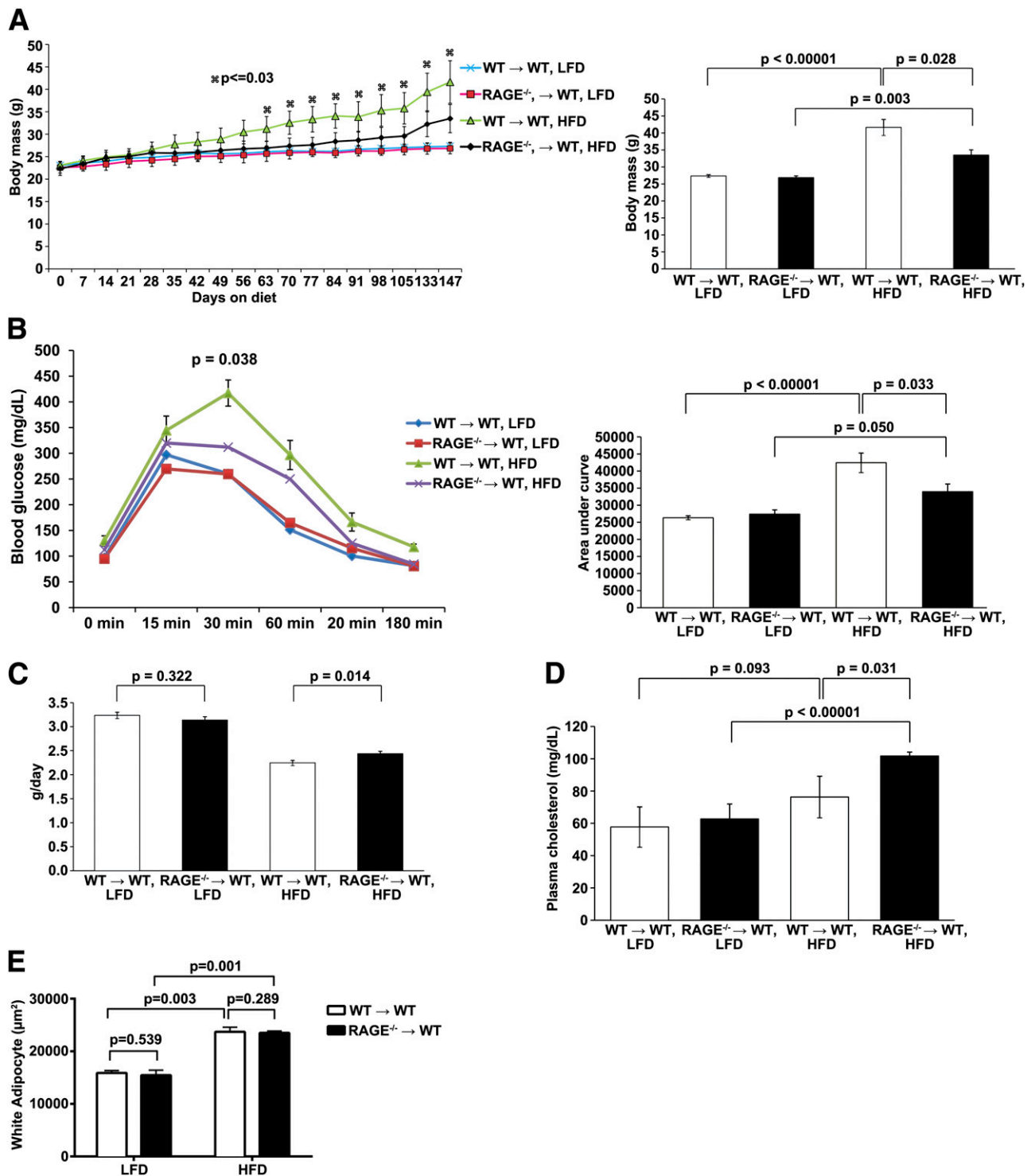
Figure 6—Bone marrow deficiency of RAGE is partially protective against HFD-induced obesity. At age 6 weeks, WT mice were subjected to lethal irradiation and reconstitution with RAGE-expressing or RAGE-deficient bone marrow. Four weeks later, mice were placed on LFD vs. HFD. A: Body mass was monitored when the mice began LFD or HFD (*left* panel) and at study end (*right* panel). B: After 21 days on the diet, a glucose tolerance test was performed. C: Food consumption was monitored in mice fed the indicated diet. D: Levels of fasting plasma cholesterol were determined in the mice at the end of study (n = 5 mice/group). E: Measurements of adipocyte size were determined in the indicated mice (n = 5 mice/group).
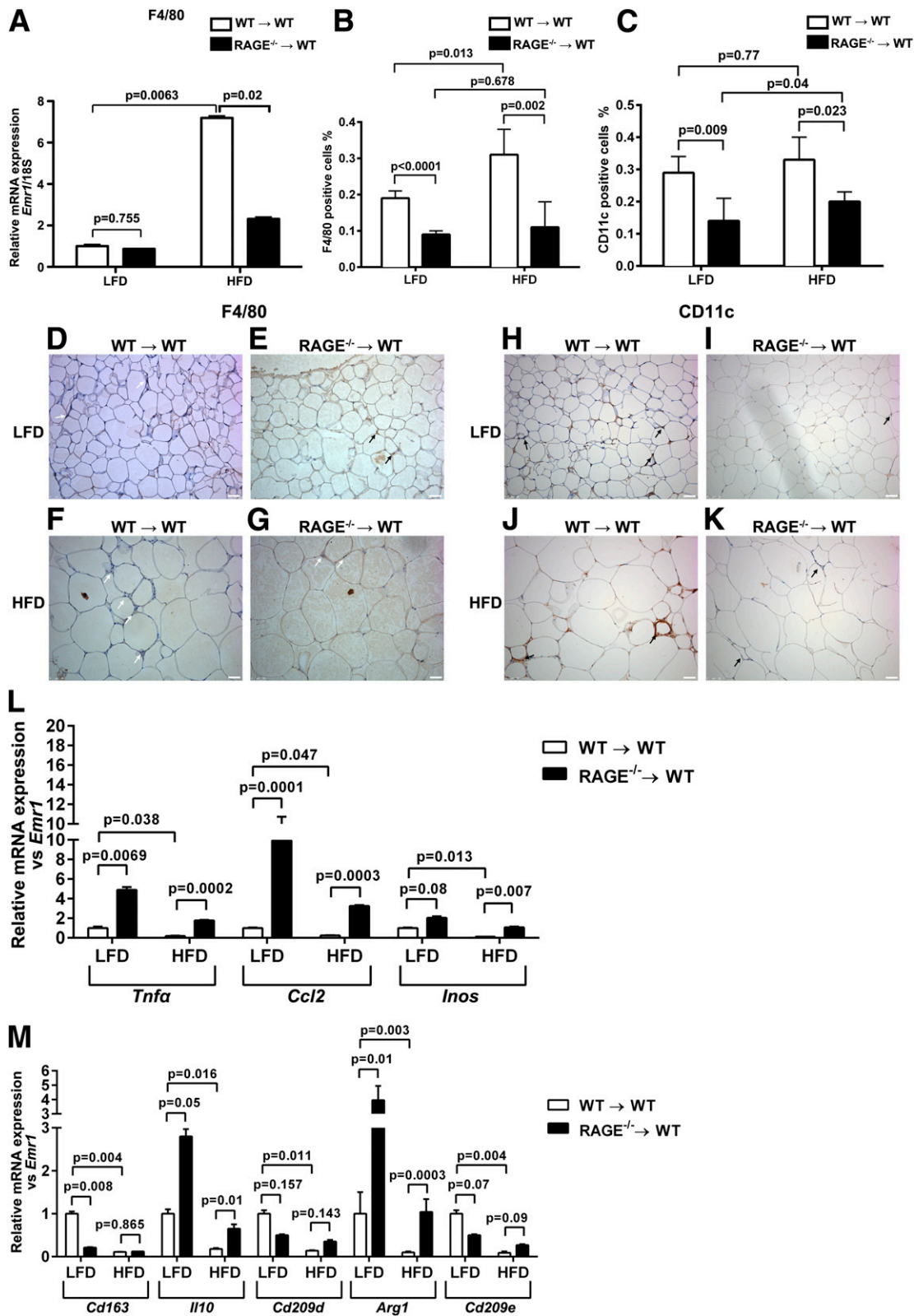
Figure 7—Deletion of bone marrow RAGE reduces macrophage *Emr1* mRNA transcripts and F4/80- and Cd11c-expressing cells and modulates M1/M2 polarization in PGAT in HFD feeding. WT mice were subjected to lethal irradiation and reconstitution with RAGE null or WT bone marrow. One month later, mice were fed LFD or HFD for 3 months. At the end of that time, PGAT was retrieved and subjected to real-time quantitative PCR for detection of *Emr1* mRNA transcripts (*A*). *B* and *C*: After 3 months on LFD or HFD, PGAT was retrieved and subjected to immunohistochemistry with anti-F4/80 (*B*) or anti-Cd11c IgG (*C*) (*n* = 5 mice/group). *D–K*: Representative images of PGAT from WT and RAGE null donor bone marrow mice at 3 months of feeding are shown for F4/80 (*D–G*) and Cd11c (*H–K*) immunoreactivity (scale bar: 40 μm). Arrows highlight F4/80- or Cd11c-expressing cells. *L* and *M*: mRNA transcripts were determined for the indicated M1 (*L*)

We examined the fate of RAGE ligands in mice treated with sRAGE beginning immediately at the time of high-fat feeding. In the PGAT of sRAGE-treated mice fed HFD, there was a trend toward lower levels of *Hmgb1* mRNA transcripts versus that observed in WT mice fed HFD and treated with vehicle ($P = 0.09$) (Supplementary Fig. 9). In the liver tissue of sRAGE-treated mice fed HFD, there was a trend toward higher levels of *Hmgb1* mRNA transcripts versus that observed in WT mice fed HFD and treated with vehicle ($P = 0.06$) (Supplementary Fig. 10). These data suggest that either distinct ligands of the receptor may be affected significantly by sRAGE or that ligand levels may not need to be decreased by measurement; rather, what may be more important is that their access to the cell surface receptor is attenuated through the sRAGE decoy effect.

Next, we tested the effects of sRAGE beginning 3 weeks after induction of HFD. Significant differences in body mass were observed between sRAGE versus vehicle-treated mice (34.4 ± 1.1 vs. 40.5 ± 1.4 g; $P < 0.05$) (Fig. 8F) without differences in food consumption (Fig. 8G).

Finally, consistent with improved insulin sensitivity and decreased inflammation in PGAT, administration of sRAGE beginning immediately at the time of high-fat feeding resulted in significantly higher PGAT mRNA transcript levels of *Slc2a4* ($P < 0.02$) (Fig. 8H) and *Adipoq* ($P < 0.000000002$) (Fig. 8I) versus vehicle-treated HFD-fed mice.

DISCUSSION

The observation that RAGE-deficient mice are resistant to diet-induced obesity and insulin resistance identifies fundamental roles for RAGE in metabolic responses, particularly to high-fat feeding. Although our original hypothesis was that RAGE would inhibit insulin signaling in HFD-fed mice through its inflammatory functions, the experiments revealed that deletion of RAGE suppressed both HFD-induced obesity and insulin resistance. Studies in agouti mice indicated that RAGE is required specifically for the metabolic response to high-fat feeding. The findings are consistent with those of Monden et al. (28) where RAGE null mice fed HFD (20% of total calories from cocoa butter and 0.15% from cholesterol) were protected from diet-induced obesity and insulin resistance and confirm the finding that RAGE contributes to regulation of adipocyte hypertrophy. In contrast, Leuner et al. (29) reported that RAGE null mice fed an HFD (60% of calories from fat) displayed greater obesity versus the WT cohort. However, Leuner et al. did not test the specific effects of RAGE expression in hematopoietic cells or the effects of RAGE antagonism. Furthermore, they did not

perform extensive metabolic phenotyping or address the nature of inflammatory cell characterization in PGAT in high-fat feeding in the context of RAGE.

Examination of the metabolic profile underscored novel roles for RAGE in energy expenditure responses to HFD. Despite equivalent food intake in WT and RAGE null mice, mice devoid of RAGE fed HFD had an increase in their metabolic rate as evidenced by increased VO_2 and body temperature. DEXA scanning revealed that RAGE null mice fed HFD displayed lower fat mass than did WT mice. Collectively, these data indicate that protection from HFD-induced obesity in RAGE null mice resulted, in large part, from increased metabolic rate. Although the absolute level of physical activity was higher in RAGE null compared with WT mice, RAGE null mice did not have an increase in physical activity between high-fat and low-fat feeding. In fact, in both WT and RAGE null mice, physical activity was lower in high-fat than in low-fat feeding. Further statistical analyses suggested that physical activity does not confound the protective effect of *Ager* deficiency on the protection against HFD-induced obesity. The finding that administration of sRAGE exerted no effect on physical activity or energy expenditure in WT mice suggests that these effects of RAGE on physical activity may result, in part, from central nervous system cues because sRAGE does not cross the blood-brain barrier. Furthermore, the intriguing finding revealing a modest, but significantly higher physical activity of lethally irradiated WT mice reconstituted with RAGE null versus WT bone marrow without any effect on energy expenditure suggests that the hematopoietic system may modulate physical activity. However, the lack of effect on body weight, food intake, and VO_2 in LFD-fed mice reconstituted with RAGE null versus WT bone marrow suggests that any effects of RAGE on motor activity are compensated for in the LFD state but not in the HFD state. Indeed, the data indicate that in high-fat feeding, mice require RAGE to gain weight. Future studies using mice with distinct tissue-specific deletion of RAGE will be of interest to fully probe the mechanisms by which RAGE might modulate physical activity and energy expenditure.

Our studies implicate RAGE-dependent inflammation in HFD-induced obesity and insulin resistance based on two principal findings. First, *Emr1* mRNA transcripts were significantly lower in the PGAT of RAGE null mice or WT mice recipients of RAGE null bone marrow than in their respective WT controls fed HFD, and numbers of F4/80- and Cd11c-expressing cells were lower when RAGE was deleted. Second, when we normalized levels of polarization marker mRNA transcripts to absolute levels of *Emr1* transcripts, a key pattern vis-à-vis RAGE was established;
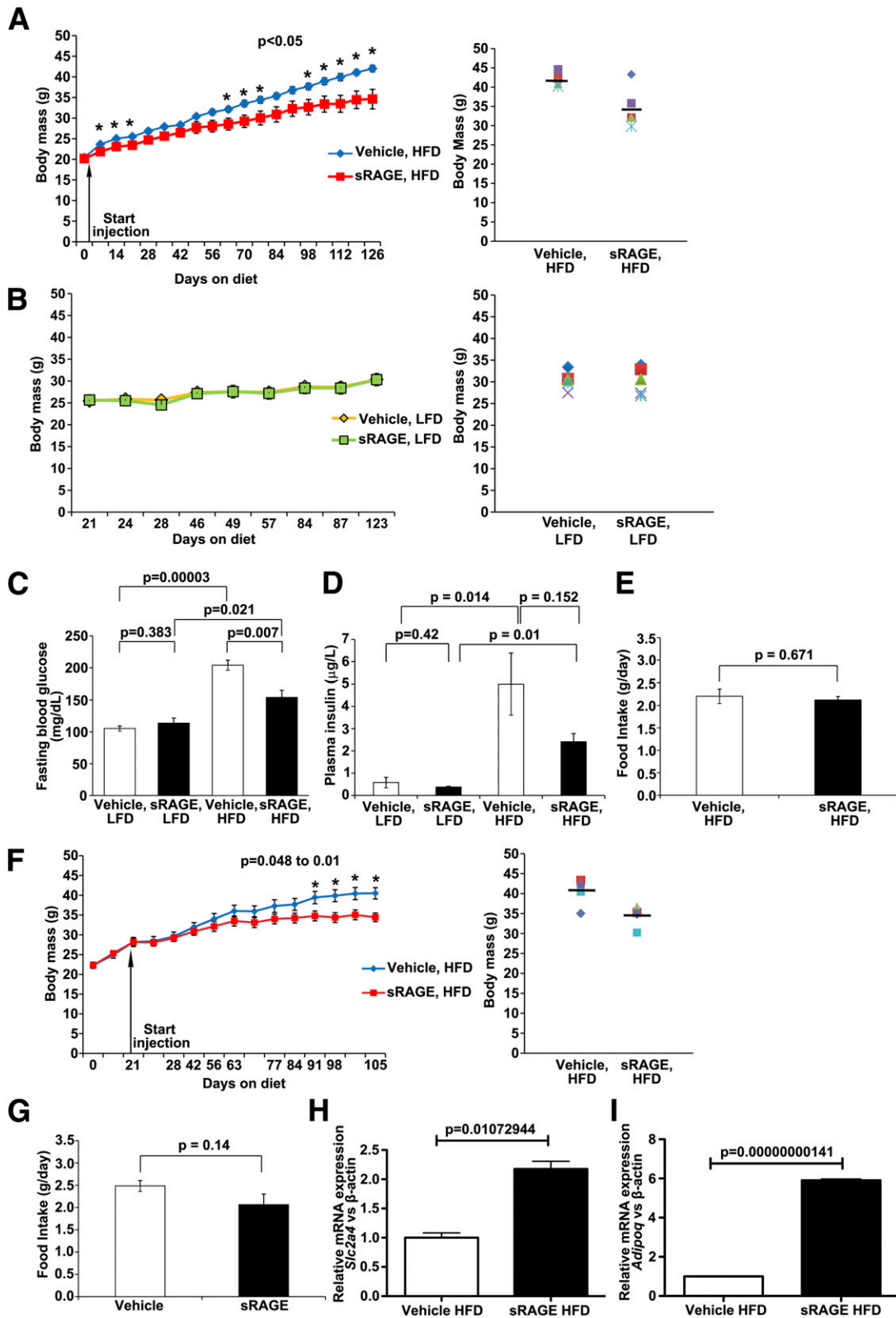
and M2 (*M*) macrophage markers and compared directly to absolute levels of *Emr1* mRNA transcripts after the 3-month diets ($n = 5$ mice/group).

Figure 8—Administration of sRAGE is partially protective against HFD-induced obesity. *A* and *B*: Prevention study. WT mice were placed on HFD (*A*) or LFD (*B*); sRAGE (100 μg/day i.p.) or vehicle PBS (equal volumes) was begun immediately at the time of diet. Body mass is shown over time (*left* panel) and by individual animals (*right* panel) (*n* = 4–5 mice/group). *C* and *D*: Fasting blood glucose (*C*) and insulin (*D*) were determined (*n* = 5 mice/group). *E*: Food consumption was measured in HFD-fed sRAGE- or PBS-treated mice (*n* = 5 mice/group). *F*: Intervention study. WT mice were placed on HFD; sRAGE (100 μg/day i.p.) or vehicle PBS (equal volumes) was begun 21 days later. Body mass is shown over time (*left* panel) and by individual animals (*right* panel) (*n* = 5 mice/group). *G*: Food consumption was measured in HFD-fed sRAGE- or PBS-treated mice (*n* = 5 mice/group). *H* and *I*: In mice treated with sRAGE vs. vehicle beginning immediately at the time

overall, either global RAGE deletion or bone marrow RAGE deletion affected macrophage polarization (30–32). RAGE deletion modestly increased levels of M1 markers and significantly increased M2 markers in the PGAT. Of note, in both global and bone marrow RAGE deficiency, a key finding was increased levels of PGAT *Il10* and *Arg1* mRNA transcripts in RAGE null mice or bone marrow, both strongly linked to insulin resistance (33–36).

The present finding that numbers of Cd11c-expressing cells were lower in PGAT when RAGE was deleted is consistent with previous work, because diphtheria toxin–mediated deletion of Cd11c resulted in significant protection against insulin resistance in HFD-fed mice, with enhanced M2 macrophage polarization, in the absence of changes in body mass (37). However, distinct studies have suggested that Cd11c expression in visceral adipose tissue macrophage subtypes may be associated with more-diverse polarization signatures. Specifically, populations of Cd11c⁺-expressing macrophages infiltrating visceral adipose tissue may display M2 polarization markers, such as Cd209A and Cd206, especially when they are lipid loaded (38). In an inducible model of lipodystrophy, mice were not obese but were significantly insulin resistant. The near complete deletion of adipocytes in this model surprisingly led to recruitment of Cd11c⁺ macrophages that largely expressed markers of M2/alternative activation, such as Cd301 and Cd206 (39–40). Hence, the specific benefit of RAGE deletion appears to have been in upregulating M2 polarization markers (especially *Il10* and *Arg1*), and perhaps suppression of Cd11-expressing cells in the PGAT in HFD, thereby establishing a relatively insulin sensitive environment. Future studies will delineate whether RAGE-dependent downregulation of M2 polarization in macrophages is accounted for by cell autonomous and/or cell–cell interactions within the PGAT. On the basis of previous work in which bone marrow–derived macrophages incubated with RAGE ligand CML-AGEs displayed downregulation of *Arg1* mRNA in a manner highly significantly prevented in RAGE null bone marrow–derived macrophages, we predict that the effects of RAGE on M2 polarization depend, at least in part, on cell-autonomous mechanisms (41).

In addition to the effect of HFD on PGAT inflammatory cell content, it has been shown that HFD feeding increases inflammation in the hypothalamus (19,42). In our studies, we examined levels of Iba1⁺ cells, a marker of activated microglia in WT and RAGE null mice fed LFD or HFD. Of note and analogous to inflammatory cell infiltration patterns in PGAT of LFD-fed RAGE null mice, on LFD, RAGE null mice displayed significantly lower numbers of Iba1⁺ cells in the hypothalamus than did WT mice fed LFD. The finding that the numbers of Iba1⁺ cells in RAGE null hypothalamus in high-fat feeding were higher than those in the hypothalamus of RAGE null mice fed LFD suggests that analysis of the pro- versus anti-inflammatory gene signatures in isolated microglia may be of interest, particularly because the RAGE null mice fed HFD did not become obese. Whether and how the numbers and inflammatory signatures of microglia and other inflammatory cells in the hypothalami of WT and RAGE null mice, both in the LFD and in the HFD states, differ may lend novel insights into mechanisms underlying physical activity and energy expenditure phenotypes in mice devoid of *Ager*.

It is notable that Monden et al. (28) showed no difference in macrophage markers between RAGE null and WT mice fed HFD, but they used Cd68 to identify macrophage cell type, which other studies have shown is not specific to macrophages in rodents and that F4/80 may be the superior macrophage marker (43). Additionally, there were differences in diet composition between the present work and that of Monden et al. The extent to which diet might have accounted for such differences in macrophage properties in visceral adipose tissue remains to be established.

A frequently considered question is what particular ligands of RAGE stimulate its action in pathological settings. We report that increased RAGE ligand *Hmgb1* in the tissues of HFD-fed mice coincided with the development of obesity. Evidence suggests links between HMGB1 and obesity. Adipose tissue of obese human subjects was found to express two times higher levels of HMGB1 protein compared with adipose tissue from lean subjects. When human adipose-derived stem cells were cultured with lipopolysaccharide, secretion of HMGB1 was greatly enhanced, suggesting that this RAGE ligand is secreted in response to inflammatory signals that typify obesity (44). Nativel et al. (45) showed that human pre-adipocytes SW872 actively secrete HMGB1 and that treatment of these cells with HMGB1 increased IL-6 production in a manner dependent on RAGE but not toll-like receptors 2 and 4. Of importance, distinct RAGE ligands in the adipose tissue might have contributed to HFD-induced obesity. For example, RAGE ligands AGEs and S100s have also been linked to obesity and insulin resistance (46,47). Irrespective of the precise RAGE ligands that accumulate in visceral adipose tissue, the present studies using sRAGE support pathogenic and not solely associative roles for RAGE ligands in obesity. Indeed, whether sRAGE is administered in a prevention or intervention mode, HFD-fed mice treated with sRAGE

of HFD feeding, PGAT was retrieved and subjected to real-time quantitative PCR for detection of *Slc2a4* (*H*) or *Adipoq* (*I*) mRNA transcripts (*n* = 4 mice/group).

appear to be protected, in part, from diet-induced obesity, thus providing early proof of concept that blocking the ligand–RAGE interaction may be a treatment strategy in these metabolic disorders.

In summary, the present data reveal that in high-fat feeding, RAGE contributes to the development of adiposity and obesity (at least in part through a reduction in metabolic rate and energy expenditure) and to the infiltration of F4/80-expressing macrophage populations into visceral adipose tissue. In the face of nutritional surplus, failure to quell RAGE responses enhances energy storage and increases adiposity. Targeting RAGE may be beneficial in the prevention of high-fat feeding–induced obesity and its metabolic consequences.

References

1. Hotamisligil GS. Inflammation and metabolic disorders. Nature 2006;444:860–867

2. Lumeng CN, Bodzin JL, Saltiel AR. Obesity induces a phenotypic switch in adipose tissue macrophage polarization. J Clin Invest 2007;117:175–184

3. Weisberg SP, McCann D, Desai M, Rosenbaum M, Leibel RL, Ferrante AW Jr. Obesity is associated with macrophage accumulation in adipose tissue. J Clin Invest 2003;112:1796–1808

4. Oh DY, Morinaga H, Talukdar S, Bae EJ, Olefsky JM. Increased macrophage migration into adipose tissue in obese mice. Diabetes 2012;61:346–354

5. Romeo GR, Lee J, Shoelson SE. Metabolic syndrome, insulin resistance, and roles of inflammation—mechanisms and therapeutic targets. Arterioscler Thromb Vasc Biol 2012;32:1771–1776

6. Ramasamy R, Yan SF, Schmidt AM. RAGE: therapeutic target and biomarker of the inflammatory response—the evidence mounts. J Leukoc Biol 2009;86:505–512

7. Kislinger T, Fu C, Huber B, et al. N(epsilon)-(carboxymethyl)lysine adducts of proteins are ligands for receptor for advanced glycation end products that activate cell signaling pathways and modulate gene expression. J Biol Chem 1999;274:31740–31749

8. Hofmann MA, Drury S, Fu C, et al. RAGE mediates a novel proinflammatory axis: a central cell surface receptor for S100/calgranulin polypeptides. Cell 1999;97:889–901

9. Taguchi A, Blood DC, del Toro G, et al. Blockade of RAGE-amphoterin signalling suppresses tumour growth and metastases. Nature 2000;405:354–360

10. Chavakis T, Bierhaus A, Al-Fakhri N, et al. The pattern recognition receptor (RAGE) is a counterreceptor for leukocyte integrins: a novel pathway for inflammatory cell recruitment. J Exp Med 2003;198:1507–1515

11. Rai V, Touré F, Chitayat S, et al. Lysophosphatidic acid targets vascular and oncogenic signaling pathways via RAGE signaling. J Exp Med 2012;209:2339–2350

12. Shanmugam N, Kim YS, Lanting L, Natarajan R. Regulation of cyclooxygenase-2 expression in monocytes by ligation of the receptor for advanced glycation end products. J Biol Chem 2003;278:34834–34844

13. Miyata T, Hori O, Zhang J, et al. The receptor for advanced glycation end products (RAGE) is a central mediator of the interaction of AGE-beta2microglobulin with human mononuclear phagocytes via an oxidant-sensitive pathway. Implications for the pathogenesis of dialysis-related amyloidosis. J Clin Invest 1996;98:1088–1094

14. Xu Y, Toure F, Qu W, et al. Advanced glycation end product (AGE)-receptor for AGE (RAGE) signaling and up-regulation of Egr-1 in hypoxic macrophages. J Biol Chem 2010;285:23233–23240

15. Zeng S, Zhang QY, Huang J, et al. Opposing roles of RAGE and Myd88 signaling in extensive liver resection. FASEB J 2012;26:882–893

16. Park L, Raman KG, Lee KJ, et al. Suppression of accelerated diabetic atherosclerosis by soluble receptor for advanced glycation endproducts. Nat Med 1998;4:1025–1031

17. Cai D, Yuan M, Frantz DF, et al. Local and systemic insulin resistance resulting from hepatic activation of IKK-beta and NF-kappaB. Nat Med 2005;11:183–190

18. Hotamisligil GS, Shargill NS, Spiegelman BM. Adipose expression of tumor necrosis factor-alpha: direct role in obesity-linked insulin resistance. Science 1993;259:87–91

19. De Souza CT, Araujo EP, Bordin S, et al. Consumption of a fat-rich diet activates a proinflammatory response and induces insulin resistance in the hypothalamus. Endocrinology 2005;146:4192–4199

20. Diani AR, Sawada GA, Hannah BA, et al. Analysis of pancreatic islet cells and hormone content in the spontaneously diabetic KKAy mouse by morphometry, immunocytochemistry and radioimmunoassay. Virchows Arch A Pathol Anal Histopathol 1987;412:53–61

21. Klaman LD, Boss O, Peroni OD, et al. Increased energy expenditure, decreased adiposity, and tissue-specific insulin sensitivity in protein-tyrosine phosphatase 1B-deficient mice. Mol Cell Biol 2000;20:5479–5489

22. Zhang Z, Zhang W, Jung DY, et al. TRPM2 Ca^{2+} channel regulates energy balance and glucose metabolism. Am J Physiol Endocrinol Metab 2012;302:E807–E816

23. Kim H-J, Higashimori T, Park S-Y, et al. Differential effects of interleukin-6 and -10 on skeletal muscle and liver insulin action in vivo. Diabetes 2004;53:1060–1067

24. Sung HK, Kim YW, Choi SJ, et al. COMP-angiopoietin-1 enhances skeletal muscle blood flow and insulin sensitivity in mice [published correction appears in Am J Physiol Endocrinol Metab 2009;297:E1233]. Am J Physiol Endocrinol Metab 2009;297:E402–E409

25. Weisberg SP, Hunter D, Huber R, et al. CCR2 modulates inflammatory and metabolic effects of high-fat feeding. J Clin Invest 2006;116:115–124

26. Guo J, Jou W, Gavrilova O, Hall KD. Persistent diet-induced obesity in male C57BL/6 mice resulting from temporary obesigenic diets. PLoS One 2009;4:e5370

27. Nguyen KD, Qiu Y, Cui X, et al. Alternatively activated macrophages produce catecholamines to sustain adaptive thermogenesis. Nature 2011;480:104–108

28. Monden M, Koyama H, Otsuka Y, et al. Receptor for advanced glycation end products regulates adipocyte hypertrophy and insulin sensitivity in mice: involvement of toll-like receptor 2. Diabetes 2013;62:478–489

29. Leuner B, Max M, Thamm K, et al. RAGE influences obesity in mice. Effects of the presence of RAGE on weight gain, AGE accumulation, and insulin levels in mice on a high fat diet. Z Gerontol Geriatr 2012;45:102–108

30.   Sica A, Mantovani A. Macrophage plasticity and polarization: in vivo veritas. J Clin Invest 2012;122:787–795

31.   Pollard JW. Trophic macrophages in development and disease. Nat Rev Immunol 2009;9:259–270

32.   Fujisaka S, Usui I, Bukhari A, et al. Regulatory mechanisms for adipose tissue M1 and M2 macrophages in diet-induced obese mice. Diabetes 2009;58: 2574–2582

33.   Hong EG, Ko HJ, Cho YR, et al. Interleukin-10 prevents diet-induced insulin resistance by attenuating macrophage and cytokine response in skeletal muscle. Diabetes 2009;58:2525–2535

34.   Cintra DE, Pauli JR, Araújo EP, et al. Interleukin-10 is a protective factor against diet-induced insulin resistance in liver. J Hepatol 2008;48:628–637

35.   Stienstra R, Duval C, Keshtkar S, van der Laak J, Kersten S, Müller M. Peroxisome proliferator-activated receptor gamma activation promotes infiltration of alternatively activated macrophages into adipose tissue. J Biol Chem 2008; 283:22620–22627

36.   Nio Y, Yamauchi T, Iwabu M, et al. Monocyte chemoattractant protein-1 (MCP-1) deficiency enhances alternatively activated M2 macrophages and ameliorates insulin resistance and fatty liver in lipoatrophic diabetic A-ZIP transgenic mice. Diabetologia 2012;55:3350–3358

37.   Patsouris D, Li P-P, Thapar D, Chapman J, Olefsky JM, Neels JG. Ablation of CD11c-positive cells normalizes insulin sensitivity in obese insulin resistant animals. Cell Metab 2008;8:301–309

38.   Prieur X, Mok CY, Velagapudi VR, et al. Differential lipid partitioning between adipocytes and tissue macrophages modulates macrophage lipotoxicity and M2/M1 polarization in obese mice. Diabetes 2011;60:797–809

39.   Fischer-Posovszky P, Wang QA, Asterholm IW, Rutkowski JM, Scherer PE. Targeted deletion of adipocytes by apoptosis leads to adipose tissue recruitment of alternatively activated M2 macrophages. Endocrinology 2011;152:3074–3081

40.   Ferrante AW Jr. Does killing adipocytes kill the bad macrophages? Endocrinology 2011;152:3304–3305

41.   Juranek JK, Geddis MS, Song F, et al. RAGE deficiency improves postinjury sciatic nerve regeneration in type 1 diabetic mice. Diabetes 2013;62:931–943

42.   Buckman LB, Hasty AH, Flaherty DK, et al. Obesity induced by a high-fat diet is associated with increased immune cell entry into the central nervous system. Brain Behav Immun 2014;35:33–42

43.   Khazen W, M'bika J-P, Tomkiewicz C, et al. Expression of macrophage-selective markers in human and rodent adipocytes. FEBS Lett 2005;579:5631–5634

44.   Gunasekaran MK, Viranaicken W, Girard AC, et al. Inflammation triggers high mobility group box 1 (HMGB1) secretion in adipose tissue, a potential link to obesity. Cytokine 2013;64:103–111

45.   Nativel B, Marimoutou M, Thon-Hon VG, et al. Soluble HMGB1 is a novel adipokine stimulating IL-6 secretion through RAGE receptor in SW872 pre-adipocyte cell line: contribution to chronic inflammation in fat tissue. PLoS One 2013;8:e76039

46.   Tan KC, Shiu SW, Wong Y, Tam X. Serum advanced glycation end products (AGEs) are associated with insulin resistance. Diabetes Metab Res Rev 2011;27: 488–492

47.   Yamaoka M, Maeda N, Nakamura S, et al. Gene expression levels of S100 protein family in blood cells are associated with insulin resistance and inflammation (peripheral blood S100 mRNAs and metabolic syndrome). Biochem Biophys Res Commun 2013;433:450–455